Latin American Journal of Solids and Structures
www.lajss.org

Early Structural Damage Assessment by Using an Improved Frequency Evaluation Algorithm

Abstract

This paper introduces a method to identify damages in beam-like structures by analyzing the natural frequency changes of the first six transversal vibration modes. A correlation between the damage location and frequency change is established for each mode separately, by considering the modal strain energy stored in that location. The mathematical relation describing this correlation is used to characterize the dynamic behavior of a beam with a damage of known position and to derive its Damage Location Indicator (DLI) as a six-term vector. The method consists in comparing the vectors describing the damage at any possible location along the beam with the Damage Signature (DS), which is achieved from the measurements that compare the beam's frequencies in healthy and damaged state. A modified Kullback-Leibler Divergence is used to assess the damage location. In order to permit early damage assessment, an improved frequency evaluation algorithm was developed. It is based on signal truncation and consequent spectral lines rearrangement, in order to accurately find the strongest spectral components. The effectiveness of the proposed method is demonstrated by simulations and experiments.

Keywords

Damage detection, Frequency shift, Modal analysis, Kullback-Leibler Divergence, Frequency evaluation, Multi-resolution

Gilbert-Rainer Gillich [a]
Nuno M. M. Maia [b]
Ion-Cornel Mituletu [a]
Zeno-Iosif Praisach [a]
Marius Tufoi [a]
Negru Ionica [a]

[a] Department of Mechanical Engineering
"Eftimie Murgu" University of Resita
320085 Resita, Romania
gr.gillich@uem.ro
mituic@yahoo.com
zpraisach@yahoo.com
m.tufoi@uem.ro
negru_ionica@yahoo.com
[b] LAETA, IDMEC, Instituto Superior Tecnico, Univ. de Lisboa, Av. Rovisco Pais, 1049-001 Lisboa, Portugal.
nmaia@dem.ist.utl.pt

http://dx.doi.org/10.1590/1679-78251795

Received 21.12.2014
Accepted 30.05.2015
Available online 07.07.2015

1 INTRODUCTION

Damage assessment is becoming an important issue in mechanical and structural engineering, since it constitutes the base regarding decision to repair or replace components. An overview about the health of structures is obtained by using the so-called global nondestructive evaluation methods. Most of these methods are based on detection and analysis of changes occurring in the vibration

characteristics of structures, because the presence of damage is signalized by changes of the modal parameters. One of the most prevalent damage detection methods considers the changes of natural frequencies, since frequency measurements can be quickly and easily conducted.

On the other hand, many researchers have reported difficulties in observing frequency changes when damage is in its early stage and detection is most desirable; see for instance Sinou (2009). An investigation regarding the minimum amount of damage that is necessary for successful detection was performed by Richardson and Mannan (1993); they concluded that the main parameters affecting the prediction are the number of vibration modes used and the measurement errors. This conclusion is valid for all vibration-based damage detection methods, irrespective of the modal parameter involved and the analysis technique. As a consequence, two directions are available to enhance the performance of the evaluation methods for early recognition of damage in structures: (∗) the use of an increased number of vibration modes and (∗∗) the improvement of the frequency resolution. Unfortunately, by increasing the number of modes, which was demonstrated as relevant, the range in which frequencies of interest are distributed enlarges, causing problems in fast and accurate frequency evaluation. Moreover, Gillich and Praisach (2014) have shown that the higher modes of a vibrating structure are rapidly damped. However, a short acquisition time leads to gross resolution, making impossible early recognition of damage. Certain doubts regarding the usefulness of frequency-based damage detection methods occur, especially in the case of small structural cracks.

In this paper a damage localization method that considers six weak-axis bending vibration modes is presented. Due to the higher number of analyzed modes, it is possible to decouple the problems of identifying the damage location and assess its severity. To ensure the identification of small frequency changes, the acquired vibration signal is post-processed by truncation with rectangular windows of different time lengths. As a result, the spectrum of each analyzed signal portion has its own frequency resolution, depending on the window time length. The superposition of all the achieved spectra results in a new spectrum with dramatically increased number of spectral lines, leading to an extremely high frequency resolution. The implementation of this signal processing algorithm in the damage detection method permits the identification of small frequency changes, and consequently early damage recognition and accurate assessment.

2 AN EXACT SOLUTION FOR THE FREQUENCY SHIFTS DUE TO A TRANSVERSAL CRACK

Damage produces a change in the dynamic behavior of structures. The effect of a transversal discontinuity is treated for instance by Bagheri et al. (2014) and Afshari and Inman (2013). They used a massless torsional spring to model the loss of rigidity due to a crack. For the two beam segments four boundary and four continuity relations are defined. The natural frequencies are individually obtained for each crack depth and location. In our previous researches we derived, by means of Finite Element Analysis, the frequency changes for numerous crack depths and locations along the beam. We considered a series of end support combinations; the results are presented, for instance, in Gillich et al. (2012) or Gillich and Praisach (2014). Typical frequency shift curves for the first three weak-axis bending vibration modes of a fixed-free beam are presented in figure 1. The curves are plotted by inserting the beam's normalized natural frequency values for two separate considered cracks that have different severities. One can first observe that the damage location producing the

highest frequency decrease is the beam's fixed end. This happens because the slice located there stores the highest amount of strain energy, while at that point the bending moment and the mode shape curvature achieve maximum values. The mathematical relation between the infinitesimal stored energy and the squared mode shape curvature is specified in equation 1.

$$dU_i(x) = \frac{1}{2} EI \left(\phi_i''(x) \right)^2 dx \tag{1}$$

where E is the Young modulus and I is the moment of inertia for the healthy beam's cross-section.

A second conclusion related to the frequency shift for the crack located at the fixed end can also be drawn. From figure 1 it can be observed that for the location $x/L = 0$, the normalized frequency shift due to a crack is similar for all weak-axis bending modes (see red circle the marks).

The same conclusion results from equation (2), which shows that the rigidity decrease due to the crack affects in equal measure all bending vibration modes, the rigidity being not linked to the mode number.

$$f_i = \frac{\lambda_i^2}{2\pi L^2} \sqrt{\frac{EI_{eq}}{\rho A}} \tag{2}$$

where λ_i is the wave number of the i-th transverse vibration mode, ρ is the mass density, A is the cross-sectional area and L the beam length.

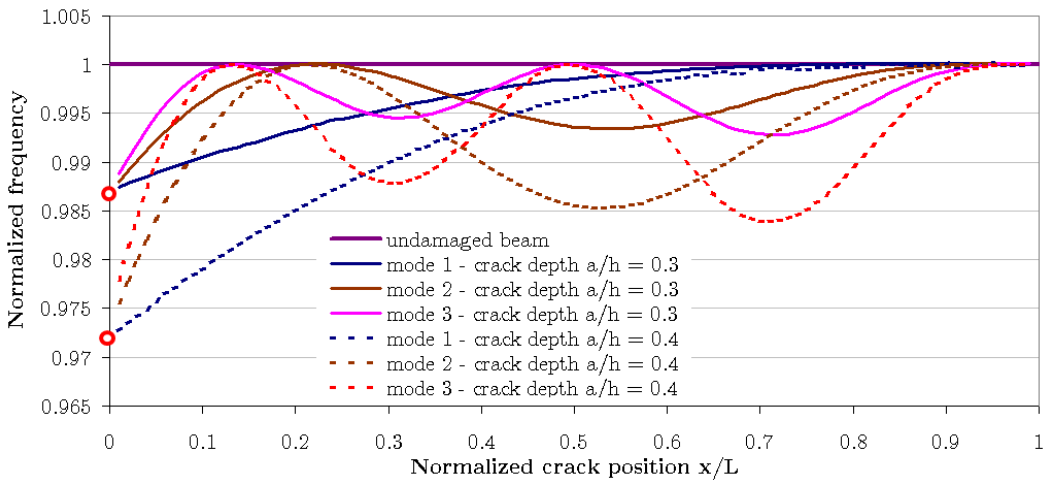

Figure 1: The frequency shift curves of the first three vibration modes of the cantilever beam, for two damage cases.

The connection between the normalized frequency shift and the damage severity is made by using Castigliano's theorem. The increased deflection of the free end due to damage, for the beam statically loaded with its own mass, reflects the apparent stored energy increase. In fact, it is an energy decrease; therefore, the original damaged beam can be replaced by an *equivalent beam* with diminished rigidity EI_{eq} due to a crack of depth a located at the fixed end. Let $\delta_U(L)$ be the deflection of

the free end for the healthy beam, having the rigidity EI, and $\delta_D(L)$ the deflection for the equivalent beam. It follows that the deflection for the healthy and damaged state are:

$$\delta_U(L) = \frac{\rho A L^4}{8EI} \qquad \text{and} \qquad \delta_D(L) = \frac{\rho A L^4}{8EI_{eq}} \tag{3}$$

Replacing alternatively EI and EI_{eq} in equation (2) leads to:

$$f_{i\_U} = \frac{\lambda_i^2}{2\pi}\sqrt{\frac{1}{8\delta_U(L)}} \qquad \text{and} \qquad f_{i\_D} = \frac{\lambda_i^2}{2\pi}\sqrt{\frac{1}{8\delta_D(L)}} \tag{4}$$

hence the normalized frequency shift due to a damage of depth a at the fixed end ($x = 0$) is:

$$\Delta\bar{f}_i(0,a) = \frac{f_{i\_U} - f_{i\_D}}{f_{i\_U}} = \frac{\frac{\lambda_i^2}{2\pi}\sqrt{\frac{1}{8\delta_U(L)}} - \frac{\lambda_i^2}{2\pi}\sqrt{\frac{1}{8\delta_D(L)}}}{\frac{\lambda_i^2}{2\pi}\sqrt{\frac{1}{8\delta_U(L)}}} = \frac{\sqrt{\delta_D(L)} - \sqrt{\delta_U(L)}}{\sqrt{\delta_D(L)}} = \gamma(a) \tag{5}$$

Moreover, from figure 1 it is obvious that the curves for the equivalent modes are quite similar, having the same allure. The amplitude differs, depending on the damage severity $\gamma(a)$, which is derived using equation (5) for each damage depth a. A visual comparison between the frequency shift curves and the corresponding normalized squared mode shape curvatures $\left[\bar{\phi}_i''(x)\right]^2 \in [0,1]$ of the healthy beam reveal a perfect concordance, justified by the fact that these curvatures reflect actually the stored energy in the slice placed at distance x from the fixed end.

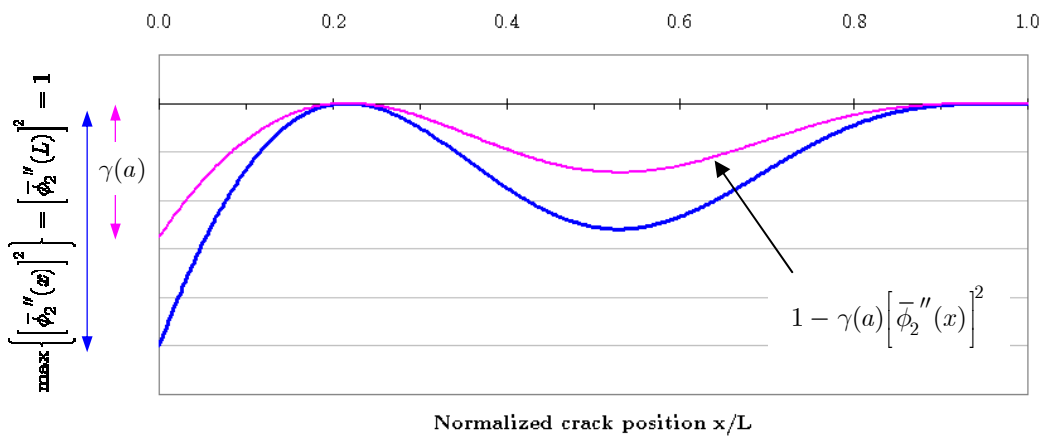

Figure 2: The normalized squared mode shape curvature for mode two (blue line) and the corresponding normalized frequency shift curve (magenta).

As a conclusion, the energy decrease is controlled by the damage severity $\gamma(a)$, equation (5), which is unique for a given damage. The location influences the frequency shift in concordance to the energy stored in the damaged slice, thus depending on the normalized squared mode shape curvature, blue line in figure 2. It means that, for a damage of depth a located at distance x from the fixed end, the normalized frequency shift is:

$$\Delta\overline{f}_i(x,a) = \gamma(a)\left[\overline{\phi}_i''(x)\right]^2 \tag{6}$$

Knowing that the frequency shift is $\Delta f_i(x,a) = f_{i\_U} \cdot \Delta\overline{f}_i(x,a)$, the mathematical relation for the natural frequencies for the transverse vibration modes of a damaged beam, $f_{i\_D}(x,a)$, in relation to the crack location x and depth a is:

$$f_{i\_D}(x,a) = f_{i\_U} - \Delta f_i(x,a) = f_{i\_U}\left\{1 - \gamma(a)\left[\overline{\phi}_i''(x)\right]^2\right\} \tag{7}$$

One should note that this simple approach is comparable with the methods using a torsional spring for which the stiffness is calculated according to the law of fracture mechanics. The difference consists in the fact that we consider the effect of the stiffness induced by a given crack at the location where the normalized squared mode shape curvature (i.e. normalized stored energy) achieve the maxima, defining in this way an *equivalent beam*. The effect of the crack location in any vibration mode is found by adjusting the severity with the local value of the healthy beam's squared curvature. Equation (7) is applicable to beams with any boundary conditions (Gillich et al., 2014.b) or in multi-span beams (Praisach et al., 2014), by simply using the proper mode shape curvature. In contrast, the current approaches need to reconsider the stiffness matrix for each crack location and/or support types and to recalculate the wave number λ_i. Another advantage of the proposed relation is the use of deflections in determining the damage severity, thus the severity is rapidly derived for any cross-section shape or even for laminar composites (Gillich et al., 2014.a). Praisach and Gillich (2013) demonstrated that equation (7) is valid for multiple cracked beams, by applying the superposition principle. An exception is the case of damages located in very closely placed cross-sections, where a stronger frequency decrease is observed.

3 A NEW DAMAGE LOCATION METHOD

Equation (6) facilitates deriving the frequency shift values for a damage located at any position along the beam, for any transverse vibration mode and beam support types. It also shows that the frequency changes do not depend on the damage depth alone. Figure 3 present, in the frequency domain, three signals derived from the free vibration of a healthy cantilever beam and the beam with two different damage scenarios. In order to highlight the phenomenon, the frequency shifts are exaggeratedly presented. One can observe that for some modes damage 1 causes a higher frequency shift, while for other modes damage 2 is responsible for this effect. Note that the amplitudes in figure 3 reflect the excitation mode, their values having no connection with the damage location or

depth. Therefore, the method presented herein takes into consideration only the frequency shifts. In the following examples six weak-axis bending vibration modes are used, which are enough to ensure a good precision. Obviously, the higher the number of considered modes, the higher the precision is.

In figure 4 the normalized frequency shifts for a cantilever beam are illustrated and the values for the normalized damage position $x/L = 0.25$ are highlighted. These values, given by the equation (6), are presented in table 1. From figure 4 and table 1 clearly results that, for any crack position, the normalized frequency shift values of several modes can be used as patterns that characterize the damage location.

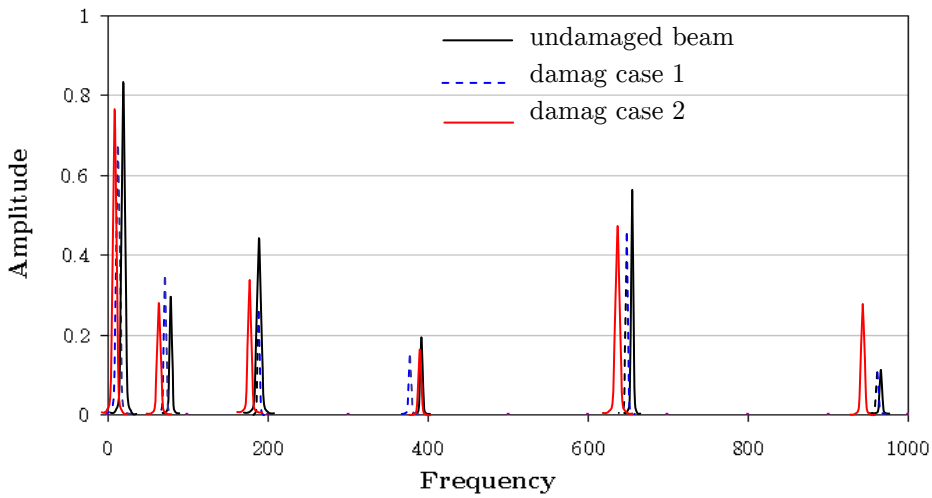

Figure 3: Comparative frequency spectra for the healthy beam and the beam with a given damage.

The series representing the pattern for a crack of depth a, located at distance x from a reference beam end, has the following mathematical expression:

$$\Delta\overline{f}_1(x,a) = \gamma(a)\cdot\left[\overline{\phi}_1{}''(x)\right]^2, \Delta\overline{f}_2(x,a) = \gamma(a)\cdot\left[\overline{\phi}_2{}''(x)\right]^2, ..., \Delta\overline{f}_6(\delta,x) = \gamma(a)\cdot\left[\overline{\phi}_6{}''(x)\right]^2 \tag{8}$$

The influence of damage depth can be removed, by eliminating $\gamma(a)$ from the sequence expressed in equation (8). It is made by dividing the normalized frequency shift values $\Delta\overline{f}_i(x,a)$ for each location x to the highest value of the sequence. The result is a set of values, independent of the damage severity. These parameters take values between 0 and 1. We denoted these series as *Damage Location Indicators* (DLI) and individual parameters as *Damage Location Coefficients* (DLC).

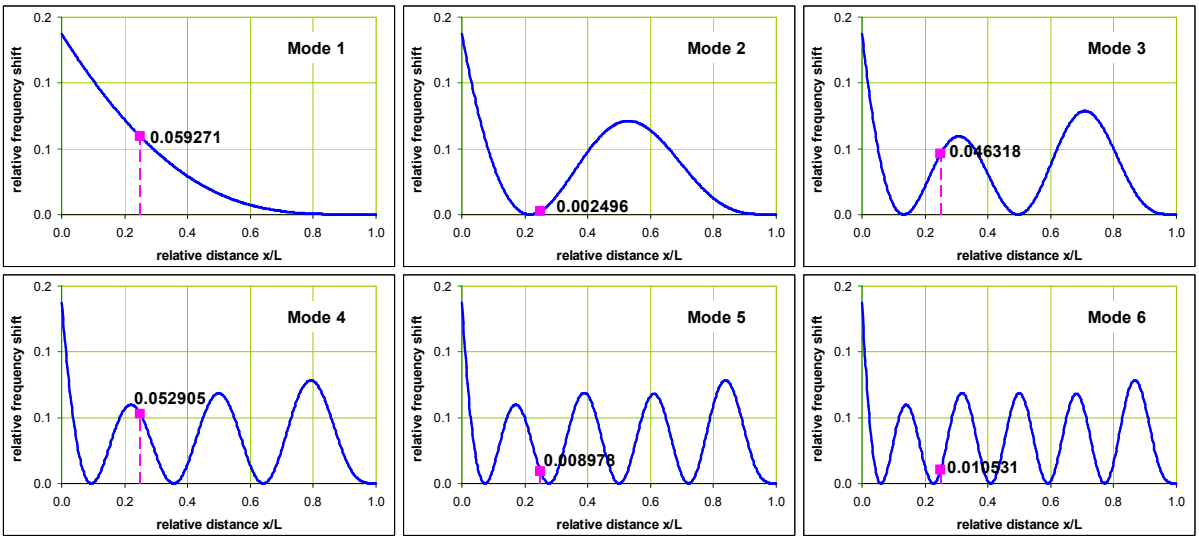

Figure 4: Frequency shift curves for the first six bending vibration modes with highlighted values for crack location $x/L = 0.25$.

For a given location x, the DLCs are expressed as:

$$\Phi_1(x) = \frac{\left[\bar{\phi}_1''(x)\right]^2}{\max\left\{\left[\bar{\phi}_i''(x)\right]^2\right\}}, \Phi_2(x) = \frac{\left[\bar{\phi}_2''(x)\right]^2}{\max\left\{\left[\bar{\phi}_i''(x)\right]^2\right\}}, \ldots, \Phi_n(x) = \frac{\left[\bar{\phi}_6''(x)\right]^2}{\max\left\{\left[\bar{\phi}_i''(x)\right]^2\right\}} \tag{9}$$

It is remarkable that the DLCs from equation (9) are obtained just using information about the beam in healthy state. A sequence of DLCs (i.e. one DLI) uniquely characterizes a location on asymmetric structures; for symmetric structures two mirrored locations have the same DLC values. For the above presented case, table 1 illustrates the DLC values for the first six vibration modes.

Normalized frequency shifts					
$\Delta\bar{f}_1$	$\Delta\bar{f}_2$	$\Delta\bar{f}_3$	$\Delta\bar{f}_4$	$\Delta\bar{f}_5$	$\Delta\bar{f}_6$
0.059271	0.002496	0.046318	0.052905	0.008978	0.010531
Damage location coefficients					
$\Phi_1(0.25)$	$\Phi_2(0.25)$	$\Phi_3(0.25)$	$\Phi_4(0.25)$	$\Phi_5(0.25)$	$\Phi_6(0.25)$
1.000000	0.042112	0.781461	0.892595	0.151474	0.177675

Table 1: Normalized frequency shift values for a crack located at $x/L = 0.25$ from the clamped end and the subsequent Damage Location Indicator as a sequence of DLCs

Figure 5 presents the values of the normalized frequency shifts (extracted from figure 4) and the consequent DLI (as a sequence of DLCs) for the cantilever beam affected by a damage located at $x/L = 0.25$. Unlike to the normalized frequency shifts, the DLI do not depend on the damage severity. One can obtain DLIs for numerous crack locations along the beam, each individualized, characterizing one location. Remarkable is that the DLCs maintain their values for a given relative damage location, irrespective to beam length, cross-section shape and damage severity.

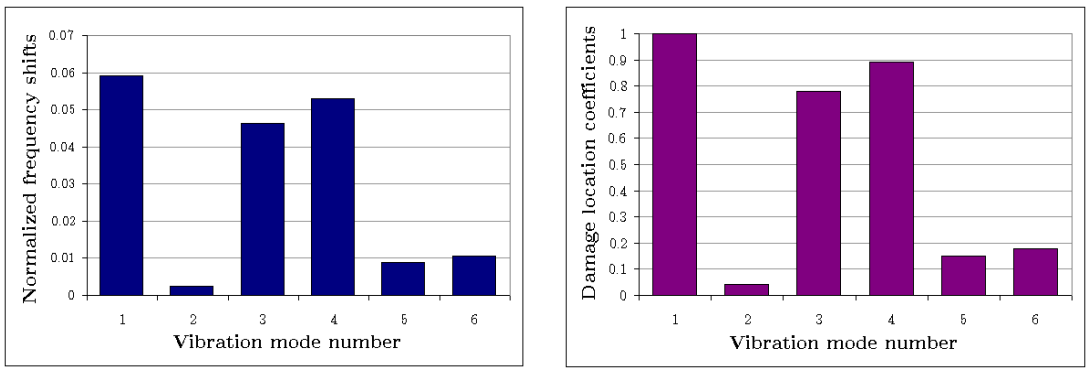

a) b)

Figure 5: The normalized frequency shifts (a) and the DLI (b) for a cantilever beam with damage at $x/L = 0.25$.

Let us now consider that $f^m_{i\_U}$ and $f^m_{i\_D}$ are the first six natural frequencies of the weak-axis bending vibration modes that have been measured on a beam in healthy state and on the same beam having one damage, respectively. The normalized frequency shifts are:

$$\Delta\overline{f}_1^{\,m} = \frac{f^m_{1-U} - f^m_{2-D}}{f^m_{1-U}},\ \Delta\overline{f}_2^{\,m} = \frac{f^m_{2-U} - f^m_{2-D}}{f^m_{1-U}},\ldots,\Delta\overline{f}_6^{\,m} = \frac{f^m_{6-U} - f^m_{6-D}}{f^m_{1-U}} \tag{10}$$

These values can be normalized by dividing them to the highest value of the series. Again, the resulted dimensionless values are severity-independent. We denote the individual parameters

$$\Psi_1 = \frac{\Delta\overline{f}_1^{\,m}}{\max(\Delta\overline{f}_i^{\,m})},\ \Psi_2 = \frac{\Delta\overline{f}_2^{\,m}}{\max(\Delta\overline{f}_i^{\,m})},\ \ldots,\Psi_n = \frac{\Delta\overline{f}_6^{\,m}}{\max(\Delta\overline{f}_i^{\,m})} \tag{11}$$

as Measured Normalized Frequency Shifts, and the series $\Psi = \left\{\Psi_1, \Psi_2, \ldots, \Psi_6\right\}$ as Damage Signature (DS). The parameters in equation (11) have a similar meaning as the DLCs; i.e. they also take values between 0 and 1.

Now, the damage localization method becomes an inverse problem. The idea is to compare the DS with numerous DLIs and to find the pair that best fits. If we consider a certain number of damage locations (for instance p), equidistantly positioned one by one along beam, any damage has an associated pattern. The analytically derived DLIs will be $\Phi_j = \left\{\Phi_1(x_j), \Phi_2(x_j), \ldots, \Phi_6(x_j)\right\}$, where $j = 1 \ldots p$. Making a similitude test between the Damage Signature Ψ and all the Damage Location Indicators Φ_j, one can find the vector Φ_j that best fits Ψ, indicating the damage location x_j. If we choose $p = 100$ possible damage locations, an error of 1% in identifying the damage location is

achieved, which is considered to fully satisfy practical applications. Obviously, the precision can be improved by increasing the number of considered locations p.

A simple algorithm was formulated in order to find the most similar vectors, derived from the Kullback-Leibler Divergence. This algorithm evaluates in the series the ratio between i parameter pairs. The idea is that, for similar values the ratio is 1 and consequently its logarithm is 0. Using a negative exponent is convenient, since it produces a dramatically increase of the lowest value and reduces to zero the all other. The value that defines the damage location is consequently highlighted. The proposed *Damage Index* is:

$$DI_{LOG-r} = \sum_{i=1}^{n} w_i \cdot \frac{1}{\Phi_{ij}} \left| \log \frac{\Phi_{ij}}{\Psi_i} \right|^{-r} \tag{12}$$

It indicates the presence of damage in the location at its highest value. Parameter w_i is a weighting factor, which takes values between 0 and 1 with the implicit value of the unit. The parameter can be diminished or even reduced to 0, in the case of getting difficulties in acquiring the natural frequency of a vibration mode or if the results are physically meaningless.

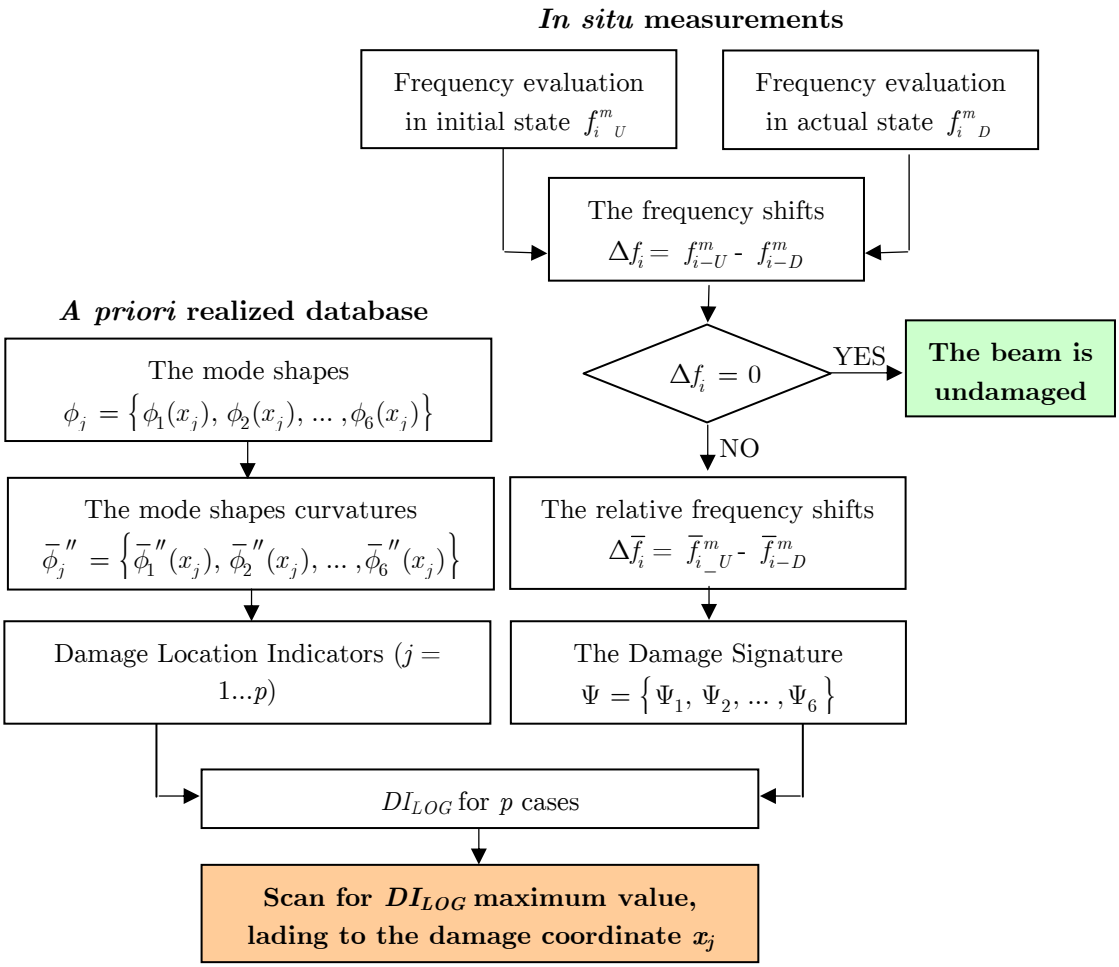

Figure 6: The damage localization algorithm

If in the initial state the beam is already damaged, the identification algorithm shows the damage evolution from this stage on, while the severity indicates the apparent energy increase from the initial state. To ensure early damage recognition it is necessary to improve the natural frequency readability, while incipient damage produces small frequency changes.

4 THE ENHANCED FREQUENCY ESTIMATION METHOD

Time-domain discrete signals achieved from vibration measurements are characterized by the time length t_S, the number of samples N_S and the sampling time Δt. Frequency spectra of these signals can be generated via a Fourier transform, the resulting values being usually presented as amplitude and phase versus frequency. In some cases it is more convenient to deal with the Power Spectral Density, which describes how the power of a signal is distributed over the different frequencies.

The frequency domain in which the information from the signal is extracted is defined by the low limit f_m that is 0, and the high limit f_M determined from the Nyquist theorem, as

$$f_M = \frac{1}{2\Delta t} = \frac{N_S - 1}{2t_S} \tag{13}$$

The frequency resolution Δf depends of the signal length in time t_S. It can be derived by using the mathematical expression

$$\Delta f = \frac{1}{t_S} = \frac{1}{\left(N_S - 1\right)\Delta t} \tag{14}$$

It defines the density of the spectral lines, thus the placing of these lines in the frequency spectrum. The aim of the frequency analysis for damage assessment is the identification of the natural frequencies as the strongest *sine* components contained in the spectrum; these components are associated with the highest frequency amplitude values. Unfortunately, if none of the spectral lines coincide to the real frequency, an inexact frequency-amplitude pair is derived. Thus, for any signal, the identified frequencies reflect the sampling strategy in higher manner than the real phenomena. Figure 7 shows the phenomenon for three sinusoids, all having the amplitude $A = 1$ mm/s^2. The first signal has a frequency $f_1 = 9.4$ Hz, the second $f_2 = 9.7$ Hz while the third has $f_3 = 10$ Hz. The considered time length is $t_S = 1$ s, and the number of samples $N_s = 1001$, resulting in $\Delta t = 0.001$ s.

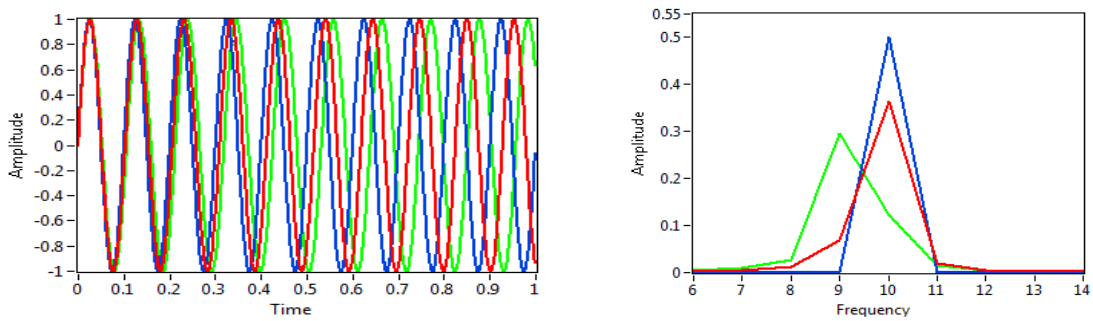

a) b)

Figure 7: The three different sine signals generated in similar condition (a) and their frequency spectrum (b); green line sine 9.4 Hz, red line sine 9.7 Hz and blue line sine 10 Hz.

From equations (13) and (14) one can derive the frequency band upper limit $f_M = 500$ Hz and the frequency resolution $\Delta f = 1$ Hz. It means that the spectral lines are distributed from 0 to 500 Hz at every unit (see figure 7.b) and consequently the amplitudes will there be indicated. For the first generated signal, the Power Spectral Density indicates the wrong frequency of 9 Hz. For the other two signals, the estimated frequency is 10 Hz; this frequency is true only for the third signal, since this frequency coincides to one of the spectral lines. One can remark that underestimation as well as an overestimation of frequency values is possible.

Note that, for the acquisition time of 1 s, the frequency resolution is 1 Hz; even if the time is increased to 10 seconds, the distance between the spectral lines is 0.1 Hz. This makes the early detection of damage using low order natural frequencies impossible, while usually the signal is altered by operational loads. For higher-order vibration modes the acquisition time is limited due to the structural damping; in this case a reasonable signal length limit is 0.5 s.

Numerous attempts concerning the improvement of frequency readability are presented in the literature. Simple techniques as zero-padding or windowing are the mostly used, see for instance Djurovic (2007) or Karjalainen and Pautero (2011). There are also more complex approaches available; Zhong-yang and Chun-yuan (2010) propose an algorithm that permits fast and accurate carrier frequency estimation, while Jacobsen and Kootsookos (2007) propose a frequency estimator based on statistical interpretation of the measured data. However, there is no certitude regarding the estimation precision, except when referring to the half of the frequency resolution. The conclusion that the current frequency evaluation methods do not distinguish very small frequency shifts should imply that the natural frequencies are little sensitive to structural changes. Actually, the frequency evaluation method is the cause of not observing early damage (i.e. small frequency changes). The goal of the proposed procedure is to precisely evaluate the frequencies, by considering the truncation of the original measured signal. If some samples are suppressed from the measured signal, a new signal is obtained with a reduced time length t_E. Nevertheless, the sampling time Δt and consequently the frequency high limit f_M do not change, but the frequency resolution Δf is modified with respect to t_E. Therefore, a frequency spectrum with redistributed spectral lines is achieved, showing different values of the amplitudes.

That means that, by the iterative decreasing of a certain number of samples from the original signal and deriving the frequency spectrum for each of them, different spectra are obtained. By superposing all these spectra a new overlapped-spectrum result, having the spectral lines number dramatically increased and the frequency resolution strongly improved.

As a reasonable limit of the iteration, this type of analysis is supposed to continue, by truncating the time signal, until one of the spectral lines is reassigned to the location where the amplitude attains a local maximum, thus indicating the real frequency component of the signal. Also, it has to be mentioned that the process must be repeated for all the frequencies that were previously considered as significant. Summarizing, the proposed algorithm is performed in four steps, as it follows:

- decreasing iteratively a certain number of time samples by applying rectangular windows to the signal;
- deriving the PSD for all truncated signals;
- superposing the achieved spectra to obtain a high resolution overlapped-spectrum;

- detecting the spectral line for which the amplitude reaches the local maximum, revealing the real frequency value.

The method offers an accurate evaluation of the frequencies if a dense spectrum is achieved. To prove that a high precision can be accomplished, four generated signals with different frequency values at a gradually increased number of digits, i.e. 10 Hz, 10.7 Hz, 10.73 Hz and 10.731 Hz, have been analyzed. Figure 8 shows a zoom of the overlapped-spectrum in the pick amplitude region. The generated frequency is in all cases easily identified at the spectral line indicating the highest amplitude, and is pointed by the cursor.

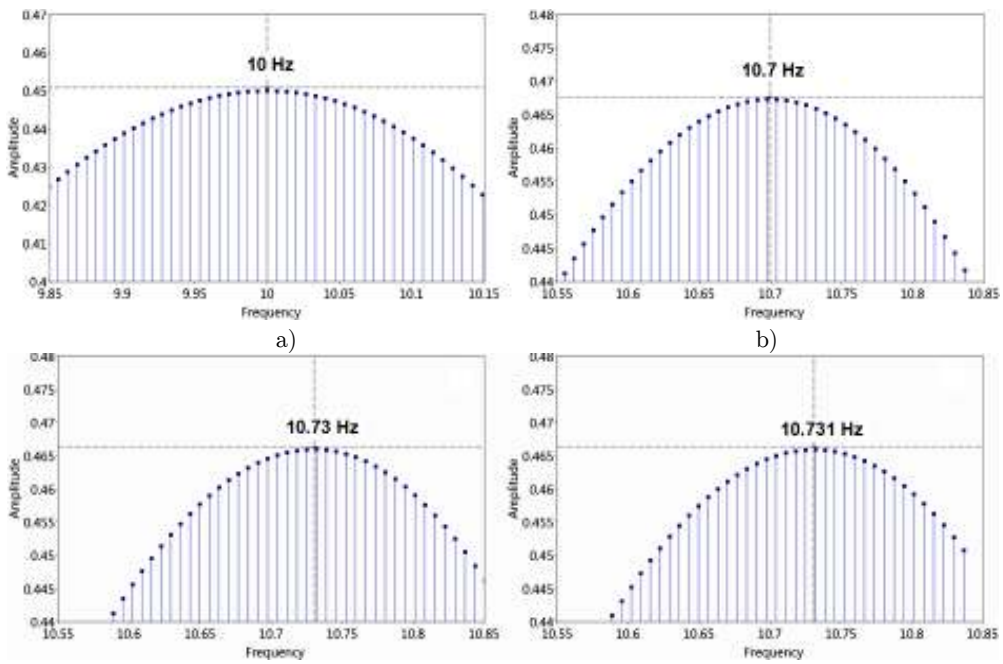

Figure 8: Accurate frequency evaluation via peak amplitude consideration.

Into the frequency range depicted in the diagrams of figure 8, considering the case of direct frequency evaluation, no more than three spectral lines can be displayed, for a given acquisition time of 10 s (which also is almost never reachable in the most cases of real applications). Thus, excepting the case of 10 Hz, in all the other cases, the spectral lines do not indicate the right frequency value. Instead, the precision of the proposed method is obviously superior, for only 1 s acquisition time, as can be seen in the above diagrams. Moreover, this precision can be adjusted via the number of samples considered at iteration and/or the time sampling rate, both are related to the same acquisition time. With the increasing of the sample number at iteration, the number of spectral lines decreases. Also, for a high sampling rate much iteration is possible and more spectral lines are available. To easy argue, let us take two examples: (i) for a low frequency the peak shape described by the amplitude high limits easy indicates the searched frequency for a less number of spectral lines as well; (ii) but for a higher frequency, the sampling rate has to be increased, in order to accomplish as much samples as possible that leads to a reasonable number of spectral lines to form a peak shape.

5 RESULTS AND DISCUSSION

In this section, the experiments conducted to validate the proposed methods are presented. A prismatic cantilevered Euler-Bernoulli beam, as shown in figure 9, was used in this study. In the undamaged state, the cantilever beam presents the following geometry: length $L = 0.7$ m, width $B = 0.05$ m and height $H = 0.005$ m. Consequently, the beam has the cross-section area $A = 250{\cdot}10^{-6}$ m^2 and the moment of inertia $I = 520.833{\cdot}10^{-12}$ m^4. The mechanical parameters of steel are: mass density $\rho = 7850$ kg/m^3; Young's modulus $E = 2.0{\cdot}10^{11}$ N/m^2 and Poisson's ratio $\mu = 0.3$.

The first six weak-axis bending vibration modes are considered. The natural frequency evaluation was performed by using a simple setup. It consists of a laptop, a NI cDAQ-9172 compact chassis with an NI 9234 signal acquisition module and a Kistler 8772 accelerometer mounted near by the free end of the beam. The structure was excited with impulse signals by hitting with a hammer. The impact location was chosen in concordance with the shapes of the different transverse modes, in order to ensure higher amplitudes to the desired frequencies.

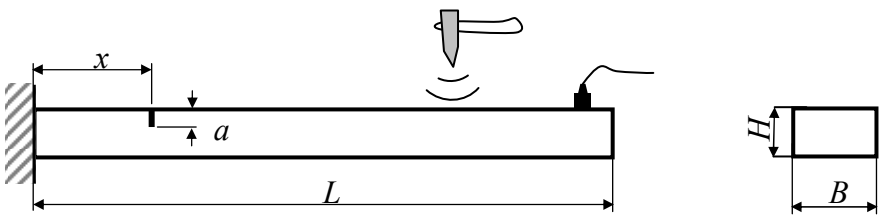

Figure 9: Cantilever beam with one damage.

The signal (see for instance the left picture in figure 10) has been acquired via a simple LabVIEW Virtual Instrument, and an ordinary frequency evaluation was performed to define the frequency domains of interest. Afterwards, the signal was analyzed via the proposed frequency evaluation procedure in order to obtain higher precision. The acquisition time is $t_S = 1$ s and the number of samples involved is $N_S = 50000$. In direct evaluation approach, increasing the number of samples the frequency upper limit increases, but without improving the frequency resolution which remains $\Delta f = 1$ Hz. Into the proposed evaluation procedure a large number of samples in the original signal ensure the fine tuning of the frequency resolution by permitting an increased number of iterations of signal truncation.

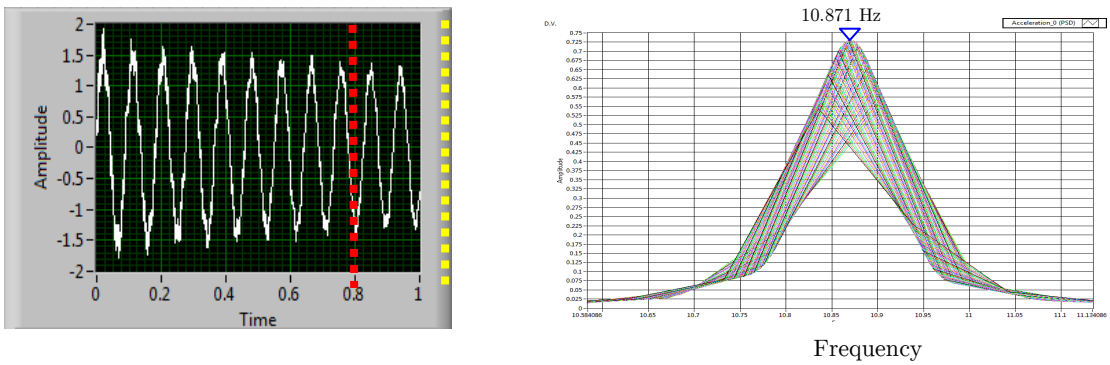

Figure 10: Acquired signal and truncation limits and the overlapped-spectrum for the frequency range corresponding to the first vibration mode, accomplished by individual spectra superposition

By applying the proposed estimation procedure the signal is iteratively truncated and numerous spectra with different frequency resolution obtained. The first time-length is 1 s (limit indicated by yellow dashed line) and is reduced until the time-length becomes 0.75 Hz (red dashed line); for all cases the PSD is derived. Superposing all the achieved spectra an overlapped-spectrum is obtained. The right picture in figure 10 illustrates this spectrum in the frequency range corresponding to the first natural frequency; the improvement of frequency estimation using the signal post-processing is evident. It is obvious that just one of the individual spectra contained in the overlapped-spectrum indicates the right frequency, this is determined in front of the highest amplitude (marked by blue triangle). From the individual spectra obtained by direct evaluation, in the range presented in figure 10, just one frequency-amplitude pair is found at 11 Hz. This shows that, without signal prost-processing, the sampling rate can significantly influence the measurement results.

The signals acquired by measurements performed on the undamaged beam, and evaluated using the proposed method, have provided the frequency values of the transverse vibration modes f_{i-U}^{m-pp} as indicated in table 2. Small differences between the results for each mode can be observed; however, the "errors" are less than 1.2%, as presented in table 3. The differences occur due to the lateral lobes of the neighbor modes, which are significant if the structure is excited in order to assure high amplitudes for these modes. To mitigate this effect, controlled excitation is requested. The possibility to capture such details confirms the proposed procedure's accuracy and availability. Unlike this, the obtained results for the undamaged beam by applying direct frequency evaluation have the same value for a given mode, even though small changes in the signals occur. This happens because, in case of direct evaluation, frequency values depend mainly on the spectral line distribution and secondary on the physical phenomenon, thus do not provide accurate results.

Mode i	Evaluated frequencies f_{i-U}^{m-pp} [Hz]				
	Test no. 1	Test no. 2	Test no. 3	Test no. 4	Test no. 5
1	10.87172	10.87113	10.87077	10.87247	10.87194
2	69.75691	69.75148	69.7548	69.75749	69.75595
3	195.2556	195.2384	195.2322	195.249	195.2463
4	383.2719	383.1344	383.2595	383.3049	383.0858
5	633.7011	634.3467	n.a.	633.4765	632.8992
6	947.3408	945.7233	947.099	n.a.	945.6263

Table 2: Natural frequencies for the undamaged beam achieved after signal post-processing.

Mode i	Evaluated frequencies f_{i-U}^{m-pp} with signal post-processing. Statistical highlights				Direct evaluated frequencies f_{i-U}^{m-d} [Hz]
	Min. f_{i-U}^{m-pp} [Hz]	Max. f_{i-U}^{m-pp} [Hz]	Error range [Hz]	Average f_{i-U}^{m-pp} [Hz]	
1	10.87247	10.87077	0.001692	10.87161	10.87202
2	69.75749	69.75148	0.006014	69.75533	69.74499
3	195.2556	195.2322	0.023454	195.2443	195.1834
4	383.3049	383.0858	0.219142	383.2113	383.187
5	634.3467	632.8992	1.447567	633.6059	633.961
6	947.3408	945.6263	1.714529	946.4474	945.2852

Table 3: Average values for the natural frequencies of the undamaged beam achieved after signal post-processing and the values extracted by direct evaluation.

From table 3 one can deduce the differences between the evaluated frequencies after post-processing and the direct achieved values f_{1-U}^{m-d}. Figure 11 shows measurement results for the first two vibration modes of the undamaged beam. For mode one, the direct evaluated frequency f_{1-U}^{m-d} is located in a central position among the extreme values achieved after post-processing, which are Min. f_{1-U}^{m-pp} and Max. f_{1-U}^{m-pp}. Value of f_{1-U}^{m-d} is therefore close to the real natural frequency value Average f_{1-U}^{m-pp} obtained for mode 1. Sampling rate fortuitously leads in this case to a credible result. Opposite, f_{2-U}^{m-d} is located far under the value Min. f_{2-U}^{m-pp}, under-evaluating the natural frequency. This confirms the importance of the proposed frequency evaluation procedure, especially for early damage recognition and assessment.

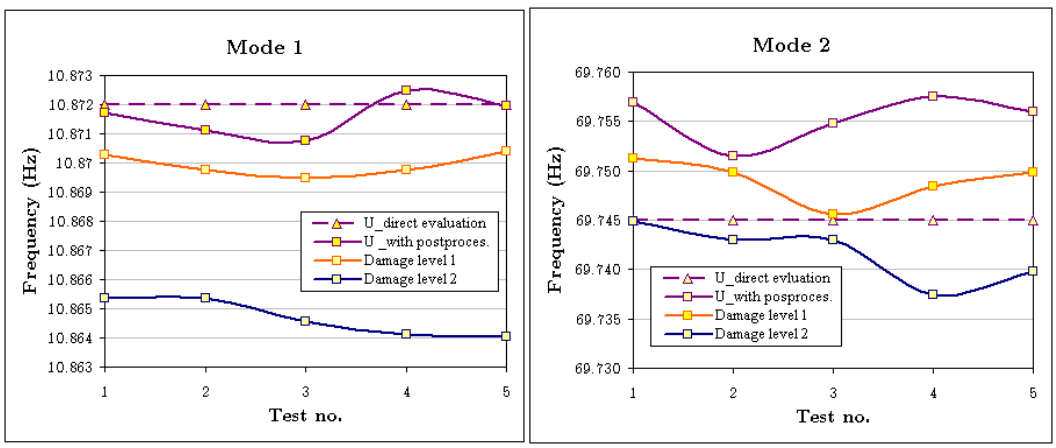

Figure 11: Evaluated frequencies of the healthy and damaged beam: vibration mode one (a) and two (b).

For the damaged cases, discontinuity was produced by a saw cut of 2 mm wide. First, a cut with depth 0.2 mm was produced; afterwards the depth was increased to 0.4 mm. The damage was placed at the distance $x = 0.077$ m, thus $x/L = 0.11$. The measured frequencies are indicated in tables 4 and 5.

Mode i	Evaluated frequencies f_{i-D1}^{m-pp} [Hz]				
	Test no. 1	Test no. 2	Test no. 3	Test no. 4	Test no. 5
1	10.87027	10.86975	10.86946	10.86975	10.8704
2	69.75124	69.7498	69.74564	69.74841	69.74986
3	195.2648	195.236	195.1966	195.2967	195.2079
4	383.2402	383.2231	383.2095	383.2308	383.1974
5	633.5656	633.7457	633.6211	633.4853	633.5999
6	946.2362	946.4702	947.0387	946.2035	946.1001

Table 4: Evaluated frequencies for the damaged beam, damage level 1 (depth 0.2 mm)

Mode i	Evaluated frequencies f_{i-D2}^{m} [Hz]				
	Test no. 1	Test no. 2	Test no. 3	Test no. 4	Test no. 5
1	10.8653	10.8654	10.8646	10.8641	10.8640
2	69.7449	69.7430	69.7430	69.7374	69.7398
3	195.2395	195.2316	195.2377	195.2369	195.2402
4	382.6900	382.5547	382.6677	382.3931	382.7244
5	633.4989	633.5638	633.4407	633.1308	633.9340
6	946.0980	946.5198	946.2171	945.9835	946.0746

Table 5: Evaluated frequencies for the damaged beam, damage level 2 (depth 0.4 mm)

As shown, the average value indicates with high accuracy the real natural frequency. Table 6 shows the frequencies of healthy beam and those corresponding to the two damage scenarios. Additionally, the two first natural frequency values are presented in Figure 11 individually for all tests. For early damage the frequency changes are insignificant and, without an accurate estimation, the damage occurrence is impossible to be detected. In addition, in case of direct frequency evaluation, an apparently increase of frequency is sometimes observed (see mode 2), introducing confusion and lack of trust in the damage detection methods.

The damage is observed even in the incipient state (cross-section reduced with less then 4%). The location is identified by comparing the Damage Signature derived using equation (11) with DLIs derived for 100 locations using equation (9). However, if the damage depth increases, a more relevant Damage Signature is obtained (see figure 12.b) and the localization process provides accurate results.

Mode i	Evaluated natural frequencies [Hz]			Damage Signature Level 2	Damage Location Indicator
	Average f_{i-U}^{m-pp}	Average f_{i-D1}^{m-pp}	Average f_{i-D2}^{m-pp}		
1	10.87161	10.86993	10.8647	1	1
2	69.75533	69.74899	69.7416	0.308624	0.249617
3	195.2443	195.2404	195.2372	0.057414	-0.0129
4	383.2113	383.2202	382.6060	0.024296	0.031499
5	633.6059	633.6035	633.5136	0.237647	0.241301
6	946.4474	946.4097	946.1786	0.445936	0.437144

Table 6: Beam natural frequencies, Damage Signature and the Damage Location Indicator for $x/L = 0.11$

The left diagram in figure 12 illustrates the Damage Index $DI_{LOG\text{-}4}$ calculated for $r = 4$ and the signature derived for damage level 2. Highest value is achieved at $x/L = 0.11$, therefore the damage location is correctly identified. The good fit between Damage Signature and Damage Location Indicator for the identified location is visible in the right diagram in figure 12. One can observe that for the extremely low damage depth $a/H = 0.04$ the signature is not relevant; however, the damage is detected and localization is possible. The difficulty appears because of the measurement errors induced by the equipment and the signal processing, but especially due to the loss of mass which affects the beam dynamics in higher manner then the stiffness reduction.

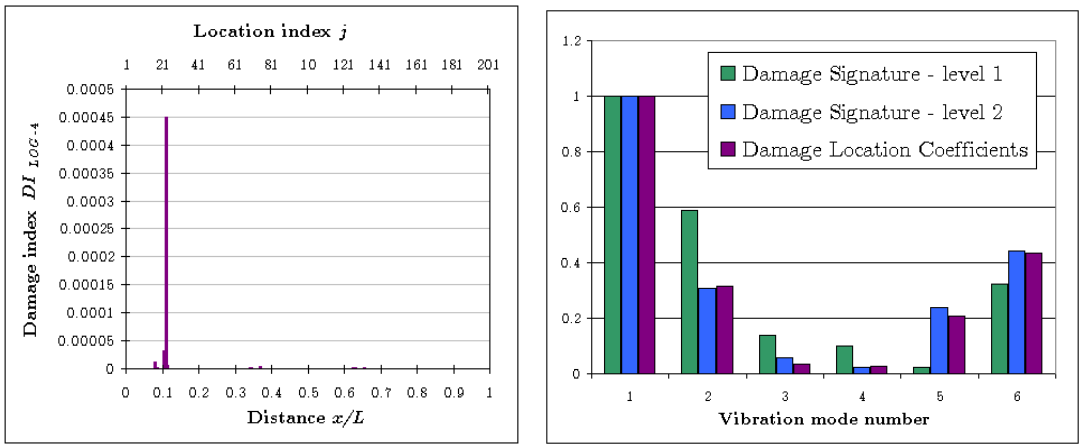

Figure 12: Similitude test for DS and DLIs - the pick value indicates the damage location at $x/L = 0.11$; and **a c**omparison between DS and DLC for the identified location and the two levels of depth.

6 CONCLUSIONS

The paper introduces a comprehensive vibration-based method for damage detection that permits accurate localization of cracks in incipient stage, even if short-time acquired vibration signals are used. To identify the damage location, two types of data are compared. The first dataset consists in the normalized frequency shifts, representing the Damage Signature, derived from measured data on the healthy and damaged structure. The second dataset involve the Damage Location Indicators, derived using equation (9) for all possible damage scenarios. A new damage index DI_{LOG} is proposed for an enhanced similarity check between the two sets of data. By using 100 equidistant damage locations to construct the database containing DLIs, the maximum error in locating damage is 1%.

It was shown that the location process and the severity assessment can be separately treated due to data normalization. Since the effect of severity is eliminated, the DS as well as the DLIs depend only on the crack location x/L. As a result, the database containing DLIs once created can be used for all beams with similar boundary conditions. For beams with variable cross-section the mode shape curvatures have to be derived.

To enhance the frequency readability, and consequently enable early damage detection, a frequency evaluation algorithm is implemented. It implies iterative truncation of the original signal, followed by a PSD analysis for each resulted segment. Superposing all obtained spectra a representation with dense spectral lines is achieved, permitting accurate frequency evaluation. Thus, a 4% cross-section reduction can be identified, while for damage of 8% the location was accurately found.

The method seems to be complicated because it makes use of numerous vibration modes, but is reliable even for this reason and in fact simple to be implemented inclusive for real structures.

Acknowledgments

The work has been funded by the Sectoral Operational Programme Human Resources Development 2007-2013 of the Ministry of European Funds through the Financial Agreement POSDRU/159/1.5/S/132395.

References

Afshari, M., Inman, D.J., (2013). Continuous crack modeling in piezoelectrically driven vibrations of an Euler–Bernoulli beam. Journal of Vibration and Control 19(3): 341–355.

Bagheri, S., Nikkar, A., Gaffarzadeh, J., (2014). Study of nonlinear vibration of Euler-Bernoulli beams by using analytical approximate techniques. Latin American Journal of Solids and Structures 11: 157 - 168.

Djurovic, I., (2007). Estimation of the Sinusoidal Signal Frequency Based on the Marginal Median DFT. IEEE Transactions on Signal Processing 55(5): 1032-1042.

Gillich, G.R., Praisach, Z.I., Iavornic, C.M., (2012). Reliable method to detect and assess damages in beams based on frequency changes. Proceedings of the ASME International Design Engineering Technical Conferences and Computers and Information in Engineering Conference, Vol. 1: 129-137.

Gillich, G. R., Praisach, Z. I., (2104). Modal identification and damage detection in beam-like structures using the power spectrum and time-frequency analysis. Signal Processing 96(Part A): 29–44.

Gillich, G.R., Praisach, Z.I., Abdel Wahab, M., Vasile, O., (2014.a) Localization of transversal cracks in sandwich beams and evaluation of their severity. Shock and Vibration 2014: Article number 607125.

Gillich, G.-R., Abdel Wahab, M., Praisach, Z.-I., Ntakpe, J.L., (2014.b). The influence of transversal crack geometry on the frequency changes of beams. International Conference on Noise and Vibration Engineering ISMA 2014. Paper ID 666

Jacobsen, E., Kootsookos, P., (2007). Fast, Accurate Frequency Estimators. IEEE Signal Processing Magazine 123.

Karjalainen, M., Pautero, T., (2001). Frequency-dependent signal windowing. Proceedings of the IEEE Workshop on Applications of Signal Processing to Audio and Acoustics (WASPAA'01): 35-38.

Praisach Z.I., Gillich G.R., (2013). Influence of multiple cracks upon the dynamic behavior of beams, Research and Applications in Structural Engineering. Mechanics and Computation - Proceedings of the 5th International Conference on Structural Engineering, Mechanics and Computation (SEMC 2013): 2199-2204.

Praisach, Z.I., Gillich, N., Negru, I., (2014). Natural Frequency Changes of Euler-Bernoulli Continuous Beams with Two Spans due to Crack Occurrence. Romanian Journal of Acoustics and Vibration 11(2): 79-82.

Richardson, M.H., Mannan, M.A., (1993). Correlating Minute Structural Faults with Changes in Modal Parameters. Proceedings of 11th MAC: 893-898.

Sinou, J.-J. (2009). A Review of Damage Detection and Health Monitoring of Mechanical Systems from Changes in the Measurement of Linear and Non-linear Vibrations. in Mechanical Vibrations: Measurement, Effects and Control: 643-702.

Zhong-yang, R., Chun-yuan, F., (2010). Fast and Accurate Frequency Estimation Algorithm for ADCP Carrier Frequency, IEEE Proceedings of 2nd International Conference on Industrial Mechatronics and Automation: 236 – 239.